

Analyst

Accepted Manuscript

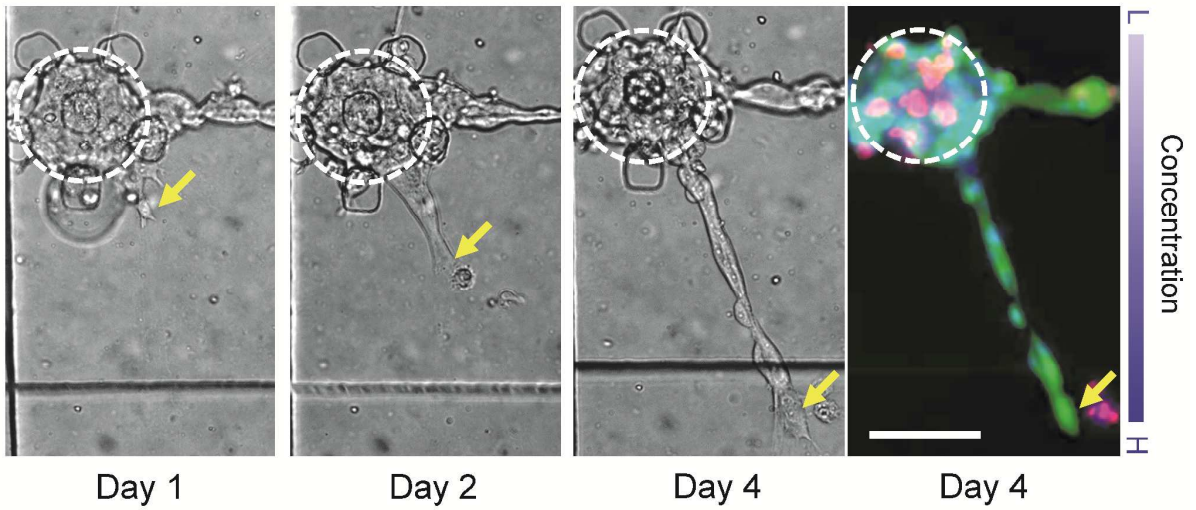


This is an *Accepted Manuscript*, which has been through the Royal Society of Chemistry peer review process and has been accepted for publication.

Accepted Manuscripts are published online shortly after acceptance, before technical editing, formatting and proof reading. Using this free service, authors can make their results available to the community, in citable form, before we publish the edited article. We will replace this *Accepted Manuscript* with the edited and formatted *Advance Article* as soon as it is available.

You can find more information about *Accepted Manuscripts* in the [Information for Authors](#).

Please note that technical editing may introduce minor changes to the text and/or graphics, which may alter content. The journal's standard [Terms & Conditions](#) and the [Ethical guidelines](#) still apply. In no event shall the Royal Society of Chemistry be held responsible for any errors or omissions in this *Accepted Manuscript* or any consequences arising from the use of any information it contains.



An *in-vitro* model of mimicking tumor microenvironments to study *in vivo*-like cancer migration and screening of inhibitors is demonstrated.

1
2
3
4
5
6
7
8
9
10
11
12
13
14
15
16
17
18
19
20
21
22
23
24
25
26
27
28
29
30
31
32
33
34
35
36
37
38
39
40
41
42
43
44
45
46
47
48
49
50
51
52
53
54
55
56
57
58
59
60

A Spatiotemporally Defined *In-Vitro* Microenvironment for Controllable Signal Delivery and Drug Screening

Ching-Te Kuo^{a,b*}, Hao-Kai Liu^{a*}, Guan-Syuan Huang^a, Chi-Hao Chang^c, Chen-Lin Chen^a, Ken-Chao Chen^a, Ruby Yun-Ju Huang^{d,e}, Ching-Hung Lin^f, Hsinyu Lee^{c**}, Chiun-Sheng Huang^{g**}, and Andrew M. Wo^{a**}

^a*Institute of Applied Mechanics, National Taiwan University, Taipei, Taiwan, R.O.C.*

^b*Institute of Atomic and Molecular Sciences, Academia Sinica, Taipei, Taiwan, R.O.C.*

^c*Department of Life Science, National Taiwan University, Taipei, Taiwan, R.O.C.*

^d*Department of Obstetrics & Gynaecology, National University Hospital, Singapore*

^e*Cancer Science Institute of Singapore, National University of Singapore, Singapore*

^f*Department of Oncology, National Taiwan University Hospital, Taipei, Taiwan, R.O.C.*

^g*Department of Surgery, National Taiwan University Hospital, Taipei, Taiwan, R.O.C.*

* These authors contributed equally to this work

** Prof. Hsinyu Lee. E-mail: hsinyu@ntu.edu.tw or

** Prof. Chiun-Sheng Huang. E-mail: huangcs@ntu.edu.tw or

** Prof. Andrew M. Wo. E-mail: andrew@iam.ntu.edu.tw

ABSTRACT

Cancer metastasis and drug resistance are important malignant tumor phenotypes that cause roughly 90% mortality in human-associated cancers. Current therapeutic strategies, however, face substantial challenges partially due to a lack of applicably pre-clinical models and drug-screening platforms. Notably, microscale and three-dimensional (3D) tissue culture platforms capable of mimicking *in vivo* microenvironments to replicate physiological conditions have become vital tools in a wide range of cellular and clinical studies. Here, we present a microfluidic device capable of mimicking a configurable tumor microenvironment to study *in vivo*-like cancer cell migration as well as screening of inhibitors on both parental tumors and migratory cells. In addition, a novel evaporation-based paper pump was demonstrated to achieve adaptable and sustainable concentration gradients up to 6 days in this model. This straightforward modeling approach allows fast patterning of a wide variety of cell types in 3D and may be further integrated into biological assays. We also demonstrated cells migration from tumor spheroids induced by an epidermal growth factor (EGF) gradient and exhibited lowered expression of epithelial marker (EpCAM) compared with parental cells, indicative of partial epithelial-mesenchymal transition (EMT) in this process. Importantly, pseudopodia

1
2
3 protrusions from the migratory cells – critical during cancer metastasis – were
4 demonstrated. Insights gained from this work offer new opportunities to achieve active
5 control of *in vitro* tumor microenvironments on demand, and may be amenable toward the
6 tailored clinical applications.
7
8
9

10 11 12 **Introduction**

13
14 Various techniques of 3D culture platforms have been established, including the use of
15 substrates coated with organic (e.g. agarose¹ and collagen²) or inorganic (e.g. poly-HEMA³
16 and hydrogel⁴) matrices, active control of cell suspension by physical forces,^{5,6}
17 layer-by-layer assemblies,⁷ and microfluidic approaches.⁸⁻¹¹ These platforms provide a
18 suitable environment for 3D culture and testing, however, challenges still remain. For
19 example, the matrix coating might interfere with the microscopic imaging and fluorometric
20 assays,¹² thus questioning the feasibility of integration with other technology, e.g.
21 microfluidics. In addition, complexity arising from the use of external systems – to
22 develop a stable concentration gradient by fluidic pumps^{11,13} – is less attractive than more
23 simplistic approaches that can be integrated with liquid handling machines.⁶ Other
24 challenges include the use of engineered nanoparticles for 3D cultures, which might have
25 biochemically and physiologically effects on the cells. Although significant progress have
26 been demonstrated in the modeling of tumor microenvironments *in vitro*,^{8,10,14} however,
27 the effect of drug on both parental tumors and the resulting migratory cells remains poorly
28 understood. Consequently, further studies are needed to elucidate the complex interaction
29 among tumor microenvironment, heterogeneity, cell migration and effects of
30 therapeutics.^{5,9,10,15-23}
31
32
33
34
35
36
37
38
39
40
41
42
43

44
45 Herein, we present a microfluidic device capable of modeling a configurable *in-vitro*
46 tumor microenvironment to probe the traits of both anti-cancer and anti-migratory drug
47 efficacy. Figure. 1a presents the *in vitro* model of the tumor microenvironment that
48 includes two top channels to simulate the epithelium and blood/lymphatic vessel,
49 respectively, a porous membrane to simulate the basement membrane, and one bottom
50 channel to simulate the stromal tissue. The microdevice was fabricated by soft lithography
51 using polydimethylsiloxane (PDMS) materials and bonded by the three-layer structures
52 (Figure. 1b). Figure. 1c shows the top features of the microdevice containing 6 solution
53 wells (4 top wells and 2 bottom wells). Tumor cells/spheroids were loaded from cell
54 channel and can be trapped deterministically then immobilized onto the defined pattern,
55
56
57
58
59
60

1
2
3
4 available for long-term observation. Chemokines/drugs were loaded from the condition
5 channel to develop a pre-determined concentration profile within the gradient channel.
6
7 Collagen scaffolds in the gradient channel simulates the stromal tissue microenvironment.
8
9 Pillars in the bottom channel enhanced the adhesion between the collagen fibers and the
10 channel walls. The Method section below provides the detail procedures. Of particular
11 feature in this device is the ability to pattern tumor spheroids and sustain their 3D
12 geometry during long-term cultures (Figure. 1d). Several reports suggested that 3D culture
13 better mimics the *in vivo*-like conditions – either in cellular morphology, mass transport
14 properties, or complex cell-matrix and cell-cell interactions – than the traditional 2D
15 environment.^{17,20,24} Therefore, our approach herein has the potential to mimic the *in-vivo*
16 3D tissue microenvironment for long-term studies, in which primary tumors always
17 maintain their 3D morphology *in vivo*. Furthermore, patterning of cells/spheroids and the
18 pre-defined chemical gradient can be easily modulated on demand by pipetting (Figure. 1c
19 and Figure. 2) over existing methods which typically need external and complicated
20 systems, thus providing a configurable tumor microenvironment at will to real-time probe
21 the traits of both anti-cancer and anti-migratory drug efficacy.
22
23
24
25
26
27
28
29
30
31
32

33 Experimental

34 Fabrication of the microfluidic device

35
36 The microdevice was fabricated as described in our earlier work²⁵ but re-designed for this
37 work. Briefly, two PDMS microchannels and a patterned porous membrane with a
38 diameter of 35 μm (for trapping of spheroids) were aligned and permanently bounded. The
39 distance between each pattern was 700 μm . The dimensions were 600- μm width \times 90- μm
40 height for the top channel and 8000- μm width \times 45- μm height for the bottom channel. The
41 length of the whole observation zone was 8.5 mm. The thickness of the membrane was 10
42 μm . Rectangular pillars, with a width of 50 μm and separated by 50 μm , were designed in
43 the bottom channel to enhance the adhesion between ECM fibers and channel walls. Holes
44 of 1 mm in diameter were mechanically drilled through the cured channels, acting as
45 fluidic inlet/outlet connections. Plastic nuts (5 mm in diameter; inner volume of 100 μl)
46 were used as solution reservoirs. Figure 1c shows the finally fabricated microdevice.
47
48
49
50
51
52
53
54
55
56
57

58 Cell culture

59 Human breast cancer cell lines MCF-7 (HTB-22, ATCC) and MDA-MB-231 (HTB-26,
60

1
2
3 ATCC) were maintained in DMEM/F12 (12400-024, GIBCO) and Leibovitz's L-15
4 (41300, GIBCO), respectively. All mediums were supplemented with 10% FBS and 1%
5 P/S. MCF-7 cells were cultured in a humidified 5% CO₂ incubator at 37°C. MDA-MB-231
6
7 cells were cultured in an atmospheric air incubator at 37°C.
8
9

10 11 12 **Preparation of Pluronic copolymers for 3D spheroid cultures**

13
14 The procedures had been reported in our previous work.²⁶ Briefly, plastic Petri dishes of
15 6-cm diameter were coated with Pluronic copolymers (1% F108 in PBS, BASF) for 1 h at
16 room temperature prior to cell loading. After washing with PBS twice, MCF-7 cells were
17 seeded by 2×10^5 cells with culture medium and incubated in a 5% CO₂ incubator at 37°.
18 Cellular spheroids were observed by microscopy daily. Prolonged spheroid cultures were
19 achieved by collection of the performed spheroids at day 5, which were sieved *via* a 70- μ m
20 cell strainer (352350, BD, Franklin Lakes, New Jersey, USA) to yield spheroids larger than
21 70 μ m in diameter.
22
23
24
25
26
27
28
29
30

31 **Configurable tumor microenvironment in the microfluidic device**

32
33 To develop an *in vivo*-like model, type I collagen gel (BD Biosciences, Franklin Lakes, NJ,
34 USA) was chosen to simulate ECM and EGF (E9644, SIGMA) as the stimulated signal
35 from stromal cells in the surrounding microenvironment, which are essential components
36 of tumor dissemination during cancer metastasis.²⁷ Prior to loading cells, the device was
37 first sterilized by UV light in a laminar-flow hood for 1 h, followed by the wash with PBS
38 twice. Loading of solutions and cells was performed by fluid height difference as
39 described.²⁵ First, collagen of 100 μ g/ml in PBS and 1% F108 were loaded within the
40 bottom channel and the cell channel, respectively, and then placed in a humidified
41 incubator at 37° overnight. Subsequently, 3D collagen scaffold was performed by loading
42 a higher collagen concentration of 1 mg/ml (pH 7.4) at 37° for 2 h, followed by washing
43 away PBS with cell culture medium. Different type sets of papers (Kimwipes, 34120,
44 KIMTECH Science) were inserted onto the outlet wells to create a stable concentration
45 gradient in a 37° incubator (details please see Figure 2 and Table S1). 100 μ l of MCF-7
46 spheroids (approximately 10 spheroids) cultured from Pluronic copolymers was loaded
47 into the cell channel and then trapped onto the cell trapping region – with a defined pattern
48 arranged by through-holes – by fluidic pressure as describes.²⁵ After 5-h culturing,
49 anti-cancer drug and/or EGF were loaded within the condition channel at day 0. The
50
51
52
53
54
55
56
57
58
59
60

cellular migration stimulated by the EGF gradient and drug responses were observed by microscopy (DM IL, Leica, Wetzlar, Germany) daily. The solutions adapted were exchanged daily with fresh ones to prevent the higher concentrated solutions due to the evaporation, thereby indicating the concentration used daily is nearly consistent. During each period of exchanging solution by manual pipetting, it would cause some disturbance of concentration gradient. The time taken to stabilize the gradient was around two hours (Figures S1 and S2). This drawback could be improved by robot machine instead of manual pipetting. The detailed method of measuring cellular responses shown in Figures. 3 and 4 is described in the Supplementary Information. In addition, fluorescence detection of epithelial cell adhesion molecule (anti-EpCAM-PE, 130-091-253, MACS; 1:100 dilution), live (calcein AM, C3100MP, Invitrogen; 7 μ M) and dead cell (propidium iodide, P4170, SIGMA; 10 μ M) staining, and nuclei staining (Hoechst 33342, Invitrogen) were performed and captured by a CCD camera (DP-70, Olympus, Shinjuku-ku, Tokyo, Japan) on an inverted microscopy. Image acquisition and analysis (i.e. the EpCAM intensity of cells) were controlled by MetaMorph software (Molecular Devices Corp., CA) using identical exposure times.

Confirmation of the concentration gradient

To confirm the concentration gradient developed in the microdevice, 0.5 mM FITC-Dextran (FD4, SIGMA; 3 ~ 5 kDa; with a similar molecular weight to EGF) in PBS was introduced from the condition channel to simulate the recombinant EGF. The experiments were conducted without cells. The concentration gradient was observed by a fluorescent microscopy and analyzed by an image software (ImageJ, 1.42q). The measured intensity (C) was normalized by the initial intensity of FITC-Dextran used (C_0) as C/C_0 .

Chemosensitivity assay

For 3D on-chip assay, paclitaxel or cisplatin was loaded within the condition channel to develop a drug gradient by the evaporation-driven flow. Upon the drug treatment, the relative cell area (top-viewed area of cellular spheroid spreading; excluding the volume effect) and the migratory cells (with numbers and migration velocities) were measured and counted daily. The relative area was defined as: average area per tumor spheroid at day n / average area per spheroid at Day 0.

mRNA expression analysis

Total RNA of cells were extracted and isolated by using TRIzol reagent (Invitrogen, Carlsbad, CA, USA). Complementary (c)DNA was synthesized from 1 μ g total RNA with a reverse-transcription polymerase chain reaction (RT-PCR). Primer sequences for real-time PCR were: GAPDH and E-cadherin (forward: 5'-TGCCCAGAAAATGAAAAAGG-3'; reverse: 5'-GTGTATGTGGCAATGCGTTC-3'), A real-time PCR with the mixture reagent SYBR-Green I (Thermo Scientific, San Diego, CA, USA) was performed in an iCycler iQ real-time detection system (Bio-Rad, Hercules, CA, USA). Each target mRNA level was evaluated and compared to the GAPDH amount as internal control from the real-time threshold cycle.

Statistical analysis

Student's t test was used to compare data from two groups of data, and ANOVA test was used to compare data from more than two groups. $p < 0.05$ was considered statistical significance. All data points were represented as mean \pm SD.

Results and discussion

Paper-based evaporation micropump

A novel paper-based evaporation pump (see Figure. 2a) was designed to realize a pre-set and stable concentration gradient over a substantial period of time (over 6 days). The piece of customized paper (details please see the Supplementary Information) essentially determines the evaporation rate, which balances the flow rate across the microchannel thereby maintaining a constant concentration within the channel. The flow velocity is proportional to the paper area (Figure. 2b and see the Table S1 for the details), in agreement with the evaporation-based equation²⁸:

$$M_e = \rho U_e = k_x A \frac{x_{A0} - x_{A\infty}}{1 - x_{A0}}$$

where M_e is the mass flux of solution into air from the solution well, ρ the density of solution, U_e the volume flux of solution, k_x the mass transfer coefficient, A the exposed area of the solution well, x_{A0} the mole fraction of solution vapor at the air/solution interface, and $x_{A\infty}$ the mole fraction of solution vapor in the bulk air of the room. We assumed that all solutions used in this approach have the same properties,

1
2
3 therefore, the volume flux U_e would be proportional to the exposed area A . In other
4
5 words, it indicates that the induced flow velocity by this approach will be corresponding to
6
7 the exposed area of the paper used, which is consistent with our results (Figure. 2b). Using
8
9 fluorescence conjugated dextran (FITC-Dextran), one can establish a configurable
10
11 concentration gradient (Figures. 2c and 2d) by using different paper area, resulting in
12
13 different flow velocity in the microchannel. Results show that this approach could generate
14
15 a particular concentration gradient, either linear or exponential profile (Figure. 2d), on
16
17 demand. The gradient profile generated from Type 3 was between Type 2 and Type 4. To
18
19 clearly identify and demonstrate the linear (Type 2) and exponential profile (Type 4), we
20
21 excluded the plot of Type 3 in Figure 2d where this exclusion should not interrogate our
22
23 results. Notably, a stable and linear concentration gradient is demonstrated within the
24
25 gradient channel, which agrees with analytical calculation, and shown to be sustainable for
26
27 up to 6 days (see Figure. 2e and the Supplementary Information for details). Although
28
29 evaporation-based micropump had been demonstrated to induce flow,^{19,29,30} however, no
30
31 study has revealed to apply this technique for the application of long-term tumor spheroid
32
33 migration/drug testing. Note that, for the first time, we utilized the paper-based
34
35 evaporation pumping for this specific application. Comparing with other existing methods,
36
37 our advantages could be more economic and flexible for the gradient generation. Although
38
39 the pumping was limited to a specific condition (37°C cell incubator) and the pumping
40
41 performance could be sensitive to the corresponding environment, the results herein should
42
43 provide a proof-of-concept demonstration for the proposed approach. In addition, the
44
45 details on the pumping performance (e.g. humidity, temperature, working solution and
46
47 other application) will be provided and discussed in the future work. Taken together, these
48
49 results suggest that this simple approach should have potential for long-term studies of
50
51 both chemical gradient and the *in vitro* tumor modeling.

52 **Migration assay**

53 To explore the particular biological attributes afforded by this defined gradient (Figure. 2e),
54
55 migration characteristics of cancer cells/spheroids under the influence of the induced
56
57 growth factor cultured in the microfluidic device was studied. Figure. 3a shows cells from
58
59 the MCF-7 spheroid migrated towards the direction of high EGF gradient during the
60
61 course of the 4-day culture. Notably, the migratory pattern of MCF-7 cells exhibits a
62
63 tether-like feature connecting the spheroid and the migrated cells, whereas other cancer

1
2
3
4
5
6
7
8
9
10
11
12
13
14
15
16
17
18
19
20
21
22
23
24
25
26
27
28
29
30
31
32
33
34
35
36
37
38
39
40
41
42
43
44
45
46
47
48
49
50
51
52
53
54
55
56
57
58
59
60

cell line – MDA-MB-231 – resulted in a discrete pattern under the same defined gradient (Figure. S3). This distinction in the migratory pattern suggests that cancer migration differs depending on the migratory cell types found, e.g. single disseminating tumor cell, collective migration, or circulating tumor microemboli (CTM; contiguous groups of tumor cells).^{31,32} This might be indicative that tumor heterogeneous plays an important role in cancer metastasis.³³ Migration/invasion of the spheroid cells through the porous membrane could not only serve as a standard assay of spheroid-based boyden chamber,³⁴ but *in-situ* create a defined chemical gradient than traditional Trans-well assay.

To further characterize the migration assay by this device, we tested MCF-7 and MDA-MB-231 breast cancer cells under a range of EGF concentrations. The detailed method for measuring the migratory cell numbers and cell migration velocities is described in the Supplementary Information and Figure. S4. Because MDA-MB-231 cells could not perform compact aggregates or spheroids by 3D on-dish cultures (data not shown), we only tested these cells with monolayer cultures, i.e. single cancer cells (MDA-MB-231 or MCF-7 cells) were cultured on the cell culture region (Figure 1c in top channel). Results show that (1) the migratory cell number and velocity increased significantly under 50 ng/ml EGF concentration from that of lower concentration (20 ng/ml) and without EGF (Figures. 3b and 3c), (2) the daily migration velocity of cells from 3D cultures was significantly higher than those from monolayer cultures (Figure. 3d), (3) the migratory cell numbers from MDA-MB-231 cells cultured in monolayer were larger than MCF-7 cells (Figure. 3e), and (4) the orientation assay shows that the migratory direction of MCF-7 cells in spheroid was responsive to the EGF gradient, whereas MCF-7 cells in monolayer were not (Figure. 3f). Moreover, the obvious difference between high EGF and no EGF gradient treatments on monolayer-cultured MDA-MB-231 cells was shown in Figure. 3g. Notably, mesenchymal-like cancer cells – MDA-MB-231– revealed more migratory properties than epithelial-like cells – MCF-7 (Figures. 3e-g), which agree with the results reported.³⁵ Furthermore, the daily migration velocity of cells – from MCF-7 cells either cultured in 3D or 2D within the microdevice – had no significant increase or decrease (from Day 2 to Day 4 in Figures 3c and 3d), suggesting that these cells might acquire an equivalent migration velocity due the near constant EGF gradient created by this work. However, the overall migration velocity and direction were significantly different between the 3D and 2D cultures (Figures. 3d and 3f). These suggests that the migratory cells – induced by the growth factor gradient – from 3D spheroids might undergo an partial EMT process, which plays a crucial role during cancer metastasis and purportedly generates

1
2
3
4
5
6
7
8
9
10
11
12
13
14
15
16
17
18
19
20
21
22
23
24
25
26
27
28
29
30
31
32
33
34
35
36
37
38
39
40
41
42
43
44
45
46
47
48
49
50
51
52
53
54
55
56
57
58
59
60

cells with properties of stem cells.^{15,36,37} Therefore, these cells might acquire an upregulated EGFR expression and be sensitive to the EGF gradient corresponding to the results (Figure. 3), which is in line with other reports on 3D cultures.^{25,36,38,39}

Anti-cancer and/or anti-migratory assay

To assess the anti-cancer and/or anti-migratory sensitivity of inhibitors on cells cultured in the microfluidic device, we treated these cells with a commonly-used chemotherapeutic drugs – paclitaxel that can be used as an inhibitor of primary tumor and cancer migration.⁴⁰ The drug was added to the condition channel, along with the EGF concentration of 50 ng/ml, thus attaining a gradient of 25.2 ng/ml/mm (Figure. 2e and Figure. S1). The average diameter of tumor spheroids trapped in the observation region was $117 \pm 23 \mu\text{m}$. Several results are noteworthy. First, the inhibition on spheroid growth and migratory ability using paclitaxel showed that a higher dose of drug treatment (100 $\mu\text{g/ml}$) may significantly increase the anti-cancer and anti-migratory sensitivities (Figures. 4a-c). The trend in Figure. 4b shows that higher drug dose (100 $\mu\text{g/ml}$) demonstrates increasing efficacy over time which was not the case at lower doses (1 and 10 $\mu\text{g/ml}$). This suggests that lower drug doses/ineffective drugs might promote or have no effect on inhibition of tumor growth, as supported by other reports on xenografted models.⁴¹ It might further imply that 3D microenvironment is critical for *in vivo*-like studies. Second, from the drug treatments on 2D-cultured MDA-MB-231 cells by paclitaxel and cisplatin, the inhibiting efficiency using paclitaxel was significantly higher than that of cisplatin (Figure. 4d), suggesting that paclitaxel is more effective on inhibiting migration than cisplatin.

Phenotypic characteristics of tumor spheroids cultured in the microdevice

The above *in vitro* migration assays suggest that the migratory or disseminated cells induced by the growth factor gradient might acquire features of EMT. To further explore these vital mechanisms in this work, we interrogated phenotypic characteristics of tumor spheroids cultured in the microdevice (Figure. 5). Results show that: (1) mRNA encoding epithelial marker was significantly downregulated (E-cadherin, ~ 0.6 -fold) compared with traditional monolayer cultures (Figure. 5a), (2) *in situ* staining with epithelial marker (EpCAM) in device shows that the migratory cells from the cellular spheroids exhibited a significant downregulation of EpCAM signal (~ 0.2 -fold) (Figure. 5b), and (3) cell

1
2
3 migration in 2D and 3D conditions were confirmed by observing their migratory
4 morphologies over 8 days, showing that the elongated multicellular protrusions formed as
5 cells migrated outward in 3D (Figure. 5c). Notably, the measurements of epithelial
6 markers (E-cadherin and EpCAM) provided further indication that these cells from
7 spheroids exist in a mesenchymal-like cell state, which more closely resemble those that
8 have undergone partial EMT than others from 2D cultures. In addition, the pseudopodia-
9 or filopodium-like protrusions – which are actin-rich with plaque of integrins – are critical
10 during cancer metastasis.^{24,42} We herein also observed these protrusions in morphology
11 either from cellular spheroid or migratory cells in 3D conditions rather than in 2D (Figure.
12 5c), indicating that cell migration depends on different mechanism in 3D. Therefore, these
13 insights gained from this work suggest that future study of metastasis should include
14 overall *in vivo*-like considerations such as co-cultures of endothelial and stromal cells, and
15 combinational chemical signals *in vivo*.^{8,23,43}
16
17
18
19
20
21
22
23
24
25
26
27

28 **Conclusions**

29
30 In summary, we have presented a microfluidic device to enable configurable tumor
31 microenvironment *in vitro* for anti-cancer and/or anti-migratory drug screenings on
32 demand. Key results demonstrated that this device may perform a stable and uniform
33 chemical gradient for long-term studies, and provide a user-friendly tool for modeling of
34 complex cancer metastasis *in vitro* and drug screening. In addition, we have revealed that
35 partial EMT and the associated morphology transition could be examined *in situ* by this
36 approach, suggesting that it could provide a useful platform to study the metastatic cascade
37 *in vitro*. As a result, these features should facilitate the long-term goal of realizing
38 “organotypic cultures” that represent tumor microenvironments towards personalized drug
39 testing.
40
41
42
43
44
45
46
47
48
49

50 **Acknowledgements**

51 Financial support from the National Science Council, Taiwan, under grants NSC
52 102-2221-E-002 -094, is gratefully acknowledged.
53
54
55
56
57
58
59
60

References

1. G. Su, Y. Zhao, J. Wei, J. Han, L. Chen, Z. Xiao, B. Chen and J. Dai, *Biomaterials*, 2013, **34**, 3215-3222.
2. J. Liu, Y. Tan, H. Zhang, Y. Zhang, P. Xu, J. Chen, Y.-C. Poh, K. Tang, N. Wang, and B. Huang, *Nature Materials*, 2012, **11**, 734-741.
3. A. Ivascu and M. Kubbies, *J. Biomol. Screen*, 2006, **11**, 922-932.
4. D.-Y. Chen, H.-J. Wei, K.-J. Lin, C.-C. Huang, C.-C. Wang, C.-T. Wu, K.-T. Chao, K.-J. Chen, Y. Chang and H.-W. Sung, *Biomaterials*, 2013, **34**, 1995-2004.
5. G. R. Souza, J. R. Molina, R. M. Raphael, M. G. Ozawa, D. J. Stark, C. S. Levin, L. F. Bronk, J. S. Ananta, J. Mandelin, M. M. Georgescu, J. A. Bankson, J. G. Gelovani, T. C. Killian, W. Arap and R. Pasqualini, *Nat. Nanotechnol.*, 2010, **5**, 291-296.
6. Y.-C. Tung, A. Y. Hsiao, S. G. Allen, Y.-S. Torisawa, M. Ho and S. Takayama, *Analyst*, 2011, **136**, 473-478.
7. B. Yuan, Y. Jin, Y. Sun, D. Wang, J. Sun, Z. Wang, W. Zhang and X. Jiang, *Adv. Mater.*, 2012, **24**, 890-896.
8. S. Chung, R. Sudo, P. J. Mack, C.-R. Wan, V. Vickerman and R. D. Kamm, *Lab Chip*, 2008, **9**, 269-275.
9. I. K. Zervantonakis, S. K. Hughes-Alford, J. L. Charest, J. S. Condeelis, F. B. Gertler and R. D. Kamm, *PNAS*, 2012, **109**, 13515-13520.
10. A. R. Aref, Ruby Y.-J. Huang, W. Yu, K.-N. Chua, W. Sun, T.-Y. Tu, J. Bai, W.-J. Sim, I. K. Zervantonakis, J. P. Thiery and R. D. Kamm, *Integr. Biol.*, 2013, **5**,
11. C. G. Sip, N. Bhattacharjee and A. Folch, *Lab Chip* DOI:10.1039/C3LC51052B (2013).
12. Y. Yoshii, A. Waki, K. Yoshida, A. Kakezuka, M. Kobayashi, H. Namiki, Y. Kuroda, Y. Kiyono, H. Yoshii, T. Furukawa, T. Asai, H. Okazawa, J. G. Gelovani and Y. Fujibayashi, *Biomaterials*, 2011, **32**, 6052-6058.
13. J. J. VanDersarl, A. M. Xu and N. A. Melosh, *Lab Chip*, 2011, **11**, 3057-3063.
14. Y.-C. Toh, C. Zhang, J. Zhang, Y. M. Khong, S. Chang, V. D. Samper, D. v. Noort, D. W. Huttmacher and H. Yu, *Lab Chip*, 2007, **7**, 302-309.
15. C. L. Chaffer and R. A. Weinberg, *Science*, 2011, **331**, 1559-1564.
16. Benbrook, D.M. Organotypic cultures represent tumor microenvironment for drug testing. *Drug Discov. Today Dis. Models* **3**, 143-148 (2006).
17. J. L. Becker and D. K. Blanchard, *Journal of Surgical Research*, 2007, **142**, 256-262.
18. K. M. Yamada and E. Cukierman, *Cell*, 2007, **130**, 601-610.
19. V. V. Abhyankar, M. W. Toepke, C. L. Cortesio, M. A. Lokuta, A. Huttenlocher and D. J. Beebe, *Lab Chip*, 2008, **8**, 1507-1515.
20. R. Derda, A. Laromaine, A. Mammoto, S. K. Y. Tang, T. Mammoto, D. E. Ingber and G. M. Whitesides, *PNAS*, 2009, **106**, 18457-1846.
21. J. Friedrich, C. Seidel, R. Ebner and L. A. Kunz-Schughart, *Nature Protocols*, 2009, **4**, 309-324.
22. D. Huh, B. D. Matthews, A. Mammoto, M. Montoya-Zavala, H. Y. Hsin and D. E. Ingber, *Science*, 2010, **328**, 1662-1668.
23. I. K. Zervantonakis, S. K. Hughes-Alford, J. L. Charest, J. S. Condeelis, F. B. Gertler and R. D. Kamm, *PNAS*, 2012, **109**, 13515-13520.
24. T.-Y. Tu, Z. Wang, J. Bai, W. Sun, W. K. Peng, Ruby Y.-J. Huang, J.-P. Thiery and R. D. Kamm, *Advanced Healthcare Materials* DOI: 10.1002/adhm.201300151 (2013).

- 1
- 2
- 3
- 4 25. C.-T. Kuo, C.-L. Chiang, Ruby Y.-J. Huang, H. Lee and A. M. Wo, *NPG Asia*
- 5 *Materials*, 2012, **4**, e27.
- 6 26. C.-T. Kuo, C.-L. Chiang, C.-H. Chang, H.-K. Liu, G.-S. Huang, Ruby Y.-J. Huang,
- 7 H. Lee, C.-S. Huang and A. M. Wo, *Biomaterials*, 2014, **35(5)**, 1562-1571.
- 8 27. E. T. Roussos, J. S. Condeelis and A. Patsialou, *Nat. Rev. Cancer*, 2011, **11**,
- 9 573-587.
- 10 28. G. M. Walker and D. J. Beebe, *Lab Chip*, 2002, **2**, 57-61.
- 11 29. C. S. Effenhauser, H. Harttig and P. Kramer, *Biomedical Microdevices*, 2002, **4**,
- 12 27-32.
- 13 30. J. M. Li, C. Liu, Z. Xu, K.P. Zhang, X. Ke, C. Y. Li and L. D. Wang. *Lab Chip*,
- 14 2011, **11**, 2785-2789.
- 15 31. J.-M. Hou, M. Krebs, T. Ward, R. Sloane, L. Priest, A. Hughes, G. Clack, M.
- 16 Ranson, F. Blackhall and C. Dive, *AM. J. Pathol.*, 2011, **178**, 989-996.
- 17 32. N. Reymond, B. Borda d'Agua and A. J. Ridley, *Nature Reviews Cancer*, 2013, **13**,
- 18 858-870.
- 19 33. N. D. Marjanovic, R. A. Weinberg and C. L. Chaffer, *Clinical Chemistry*, 2012, **59**,
- 20 168-179.
- 21 34. N. Kramer, A. Walzl, C. Unger, M. Rosner, G. Krupitza, M. Hengstschlager and H.
- 22 Dolznig, *Mutation Research*, 2013, **752**, 10-24.
- 23 35. F. Tang, R. Zhang, Y. He, M. Zou, L. Guo and T. Xi, *PLOS ONE*, 2012, **7**, e35435.
- 24 36. J. P. Thiery, H. Acloque, Ruby Y.-J. Huang and M. A. Nieto, *Cell*, 2009, **139**,
- 25 871-890.
- 26 37. S. A. Mani, W. Guo, M.-J. Liao, E. N. Eaton, A. Ayyanan, A. Y. Zhou, M. Brooks, F.
- 27 Reinhard, C. C. Zhang, M. Shipitsin, L. L. Campbell, K. Polyak, C. Brisken, J.
- 28 Yang and R. A. Weinberg, *Cell*, 2008, **133**, 704-715.
- 29 38. J. M. Lee, P. Mhawech-Fauceglia, N. Lee, L. C. Parsanian, Y. G. Lin, S. A. Gayther
- 30 and K. Lawrenson, *Laboratory Investigation*, 2013, 1-15.
- 31 39. D. Hanahan and R. A. Weinberg, *Cell*, 2011, **144**, 646-674.
- 32 40. G. Bocci, A. D. Paolo and R. Danesi, *Angiogenesis*, 2013, **16**, 481-492.
- 33 41. D. Decaudin, *Anti-Cancer Drugs*, 2011, **22**, 827-841.
- 34 42. T. Shibue, M. W. Brooks, M. F. Inan, F. Reinhardt and R. A. Weinberg, *Cancer*
- 35 *Discovery*, 2012, **2**, 706-721.
- 36 43. W. J. Polacheck, I. K. Zervantonakis and R. D. Kamm, *Cell. Mol. Life Sci.*, 2012,
- 37 **70**, 1335-1356.
- 38
- 39
- 40
- 41
- 42
- 43
- 44
- 45
- 46
- 47
- 48
- 49
- 50
- 51
- 52
- 53
- 54
- 55
- 56
- 57
- 58
- 59
- 60

Figure Captions

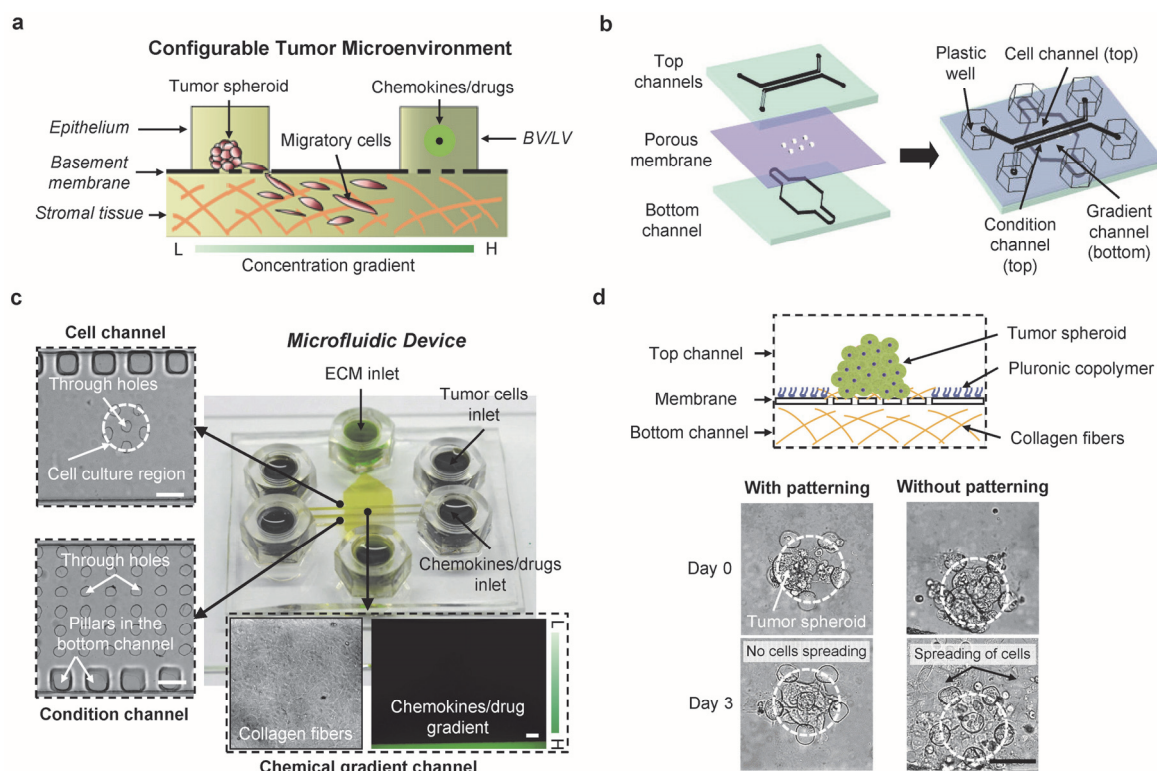


Fig. 1 Design of the microfluidic device. (a) A schematic showing the experimental design: (1) the stromal tissue was modeled using 3D ECM scaffold in the bottom of the microdevice; (2) a tumor spheroid was grown onto the basement membrane surface in the epithelium; (3) cells may acquire metastatic potential and migrate to a distant site due to a stable concentration gradient of solvable factors, generated from the configurable tumor microenvironment. BL/LV, blood vessels/lymphatic vessels. (b) Illustration of the overall configuration with two top channels (cell channel as *epithelium* and condition channel as *BV/LV*, respectively) and one bottom channel (gradient channel as *stromal tissue*) sandwiching the cell-supporting membrane (*basement membrane*) with fabricated through-holes. Plastic wells were used as solution reservoirs. (c) Micrographs of various portions of the fabricated device. (d) Results obtained with Pluronic copolymer patterning and those obtained without patterning. Scale bars, 100 μm .

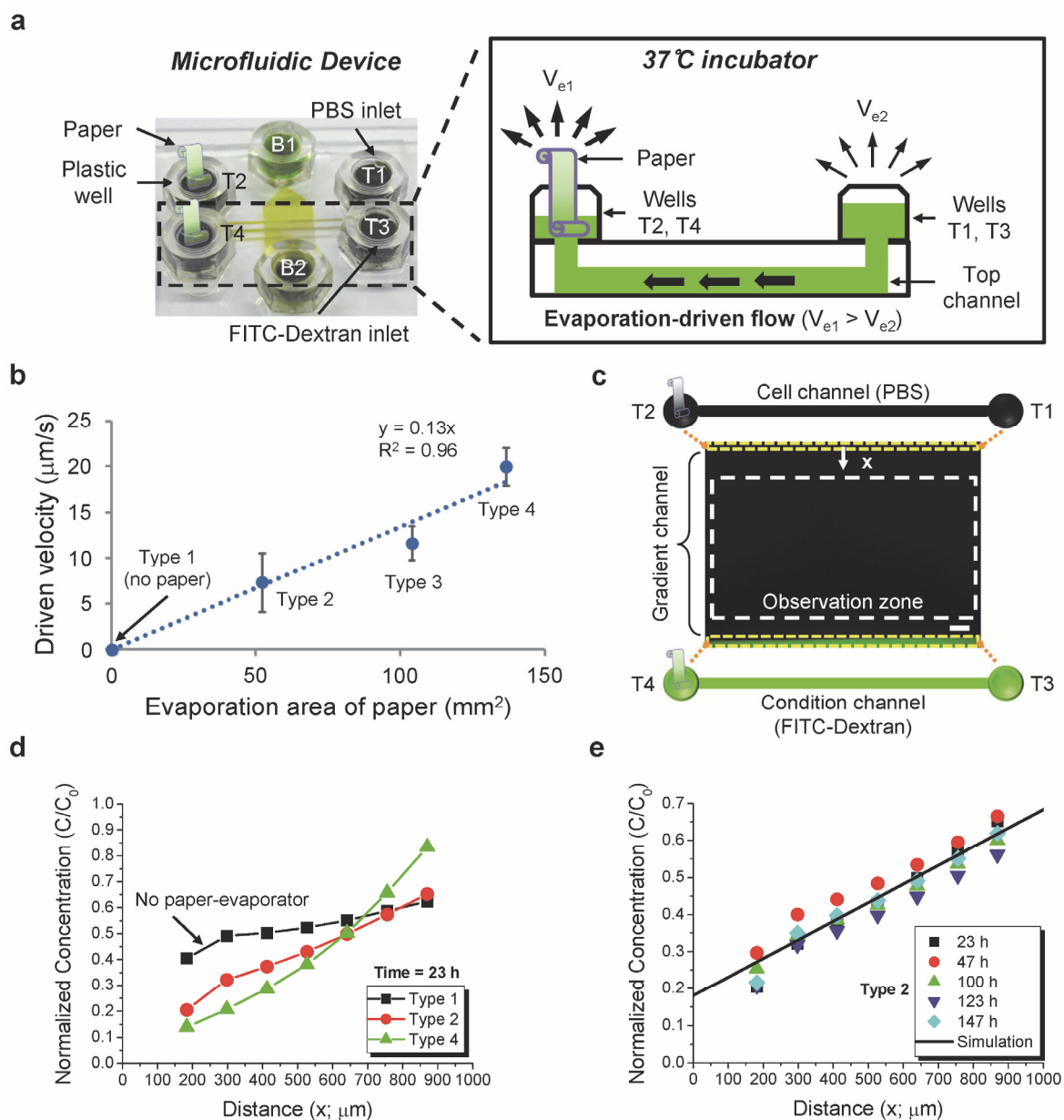


Fig. 2 A spatiotemporally defined 3D microenvironment. (a) Schematic showing the experimental setup to enable a stable concentration gradient in the microdevice. PBS was loaded from the cell channel and FITC-Dextran was loaded from the condition channel. The heights of solutions in the plastic wells were kept the same. Customized papers were inserted into the outlet wells of the two top channels to increase an additional evaporation area. This device was then placed in a cell culture incubator at 37°C. After incubation, it will generate two equivalent evaporation-driven flows in the two top channels due to the asymmetric and competitive evaporation rates, i.e. $V_{e1} > V_{e2}$. T1 ~ T4 and B1 ~ B2 denote the well number in the top and bottom channels, respectively. (b) Driven velocity versus evaporation area of the customized papers. Type 1: without paper; Type 2: 52.32 mm^2 ; Type 3: 104.16 mm^2 ; Type 4: 136.71 mm^2 . Each point represents an average of $n = 4$ for

1
2
3
4 each condition. (c) A concentration gradient was developed in the gradient channel (bottom
5 layer) of this device. The yellow-dashed rectangles represent the cell and condition
6 channels, respectively, in the top layer of the device. The dashed rectangle (white color)
7 denotes the observation zone. The “x” indicates the distance of measurement. (d) Either
8 linear or exponential concentration profile can be developed on demand by different types
9 of customized papers. C_0 is the initial fluorescent intensity of FITC-Dextran and C is the
10 measured intensity. (e) A linear concentration profile was maintained within the 3D
11 collagen fiber-filled bottom channel for up to 6 days by using Type 2 paper configuration.
12
13
14
15
16
17
18 Scale bar, 100 μm .

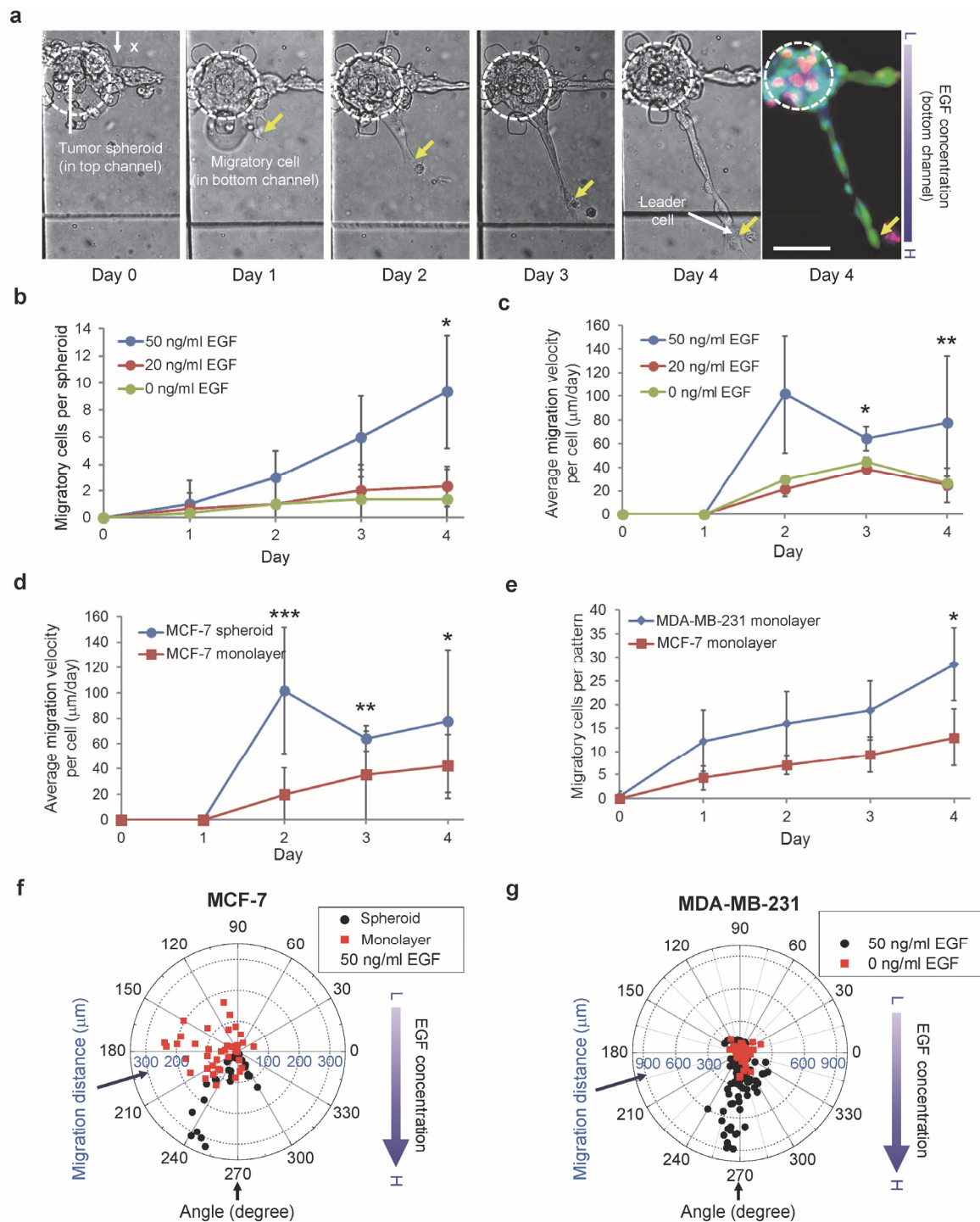


Fig. 3 Growth factor-induced cancer cell migration. (a) Micrographs showing time sequence of a cell migration from MCF-7 tumor spheroid under the growth factor gradient of 50 ng/ml EGF. The yellow arrows indicate the extent of migratory cells. Live cell staining (calcein AM, green), dead cell staining (propidium iodide, red), and Hoechst nuclear staining (blue) were applied at Day 4. The dashed circle illustrates the initial cell trapping region. Scale bar, 100 μm . (b) and (c) Number of migratory cells per MCF-7 tumor spheroid and the average migration velocity per cell under different concentrations

1
2
3 of EGF. (d) The comparison of average migration velocity between MCF-7 spheroids (3D)
4 and single MCF-7 cells (monolayer) cultured in the device. (e) The monolayer migration
5 results between MCF-7 and MDA-MB-231 breast cancer cells. (f) Oriented migration of
6 MCF-7 cells cultured in 3D and 2D under an EGF gradient of 50 ng/ml. (g) Oriented
7 migration of MDA-MB-231 cultured in 2D under EGF gradients of 0 and 50 ng/ml. Each
8 point represents an average with $n = 3 \sim 5$ for (b) and (e), and $n = 3 \sim 71$ for (c) and (d).
9
10
11
12
13
14
15
16
17
18
19
20
21
22
23
24
25
26
27
28
29
30
31
32
33
34
35
36
37
38
39
40
41
42
43
44
45
46
47
48
49
50
51
52
53
54
55
56
57
58
59
60

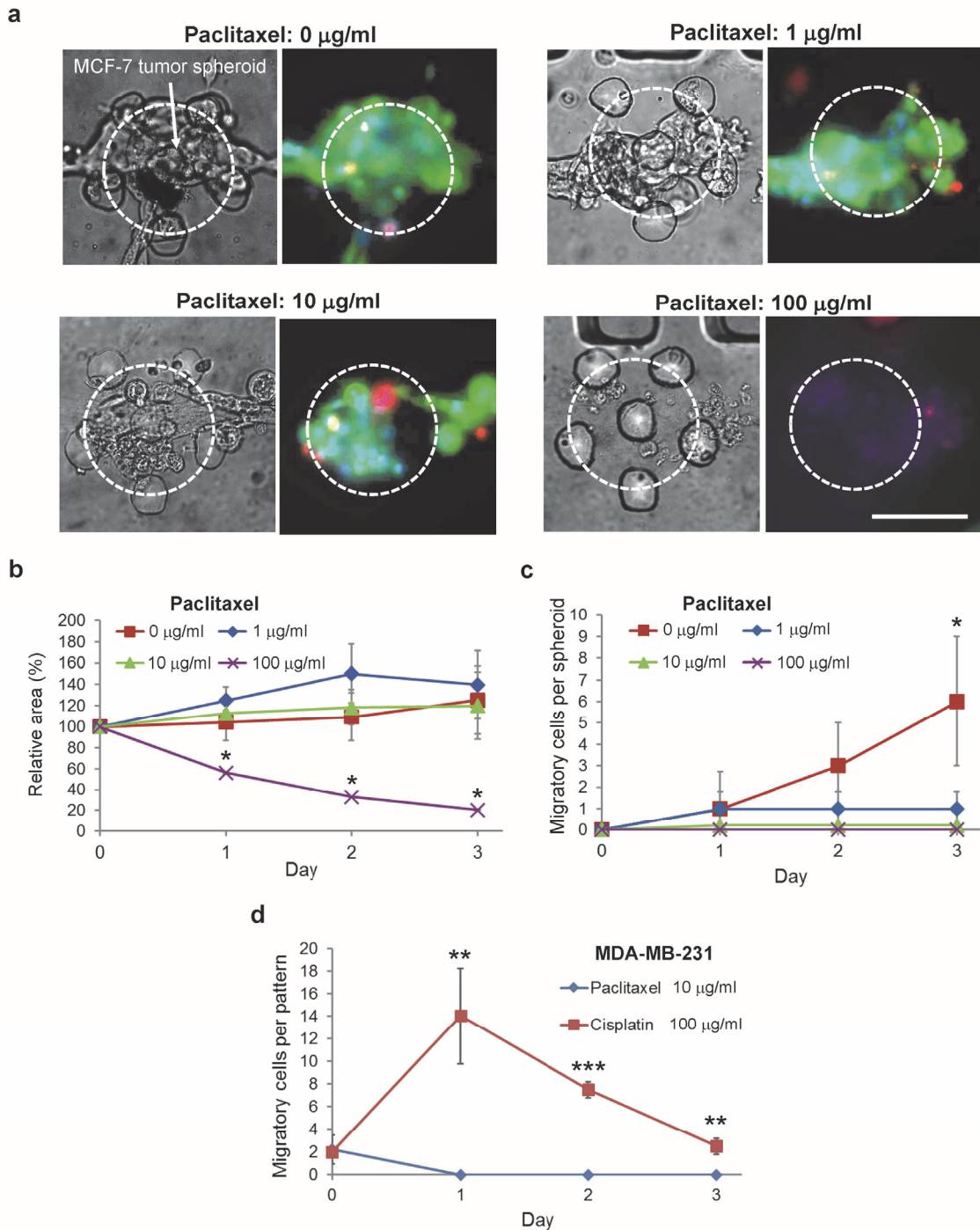


Fig. 4 Anti-cancer and anti-migratory drug screenings (mixture of EGF and paclitaxel/cisplatin are loaded in both wells T3 and T4). (a) Morphology of MCF-7 spheroids under a range of paclitaxel concentrations at Day 3. Live cells and dead cells are indicated by a green dye (calcein AM) and a red dye (propidium iodide), respectively. Nucleus was stained with Hoechst dye (blue). Scale bar, 100 μm . (b) Relative area (average area per MCF-7 spheroid / average area per MCF-7 spheroid at Day 0) over the course of 3-day culture treated with paclitaxel of various concentrations. (c) The number of migratory cells per MCF-7 spheroid over the 3-day culture treated with paclitaxel of

C. T. Kuo et al. *Manuscript for Analyst* *page 18*

1
2
3 various concentrations. (d) The number of migratory cells per MDA-MB-231 pattern
4 treated with paclitaxel of 10 $\mu\text{g/ml}$ and cisplatin of 100 $\mu\text{g/ml}$ over the 3-day culture. Each
5 point represents an average with $n = 3 \sim 4$.
6
7
8
9
10
11
12
13
14
15
16
17
18
19
20
21
22
23
24
25
26
27
28
29
30
31
32
33
34
35
36
37
38
39
40
41
42
43
44
45
46
47
48
49
50
51
52
53
54
55
56
57
58
59
60

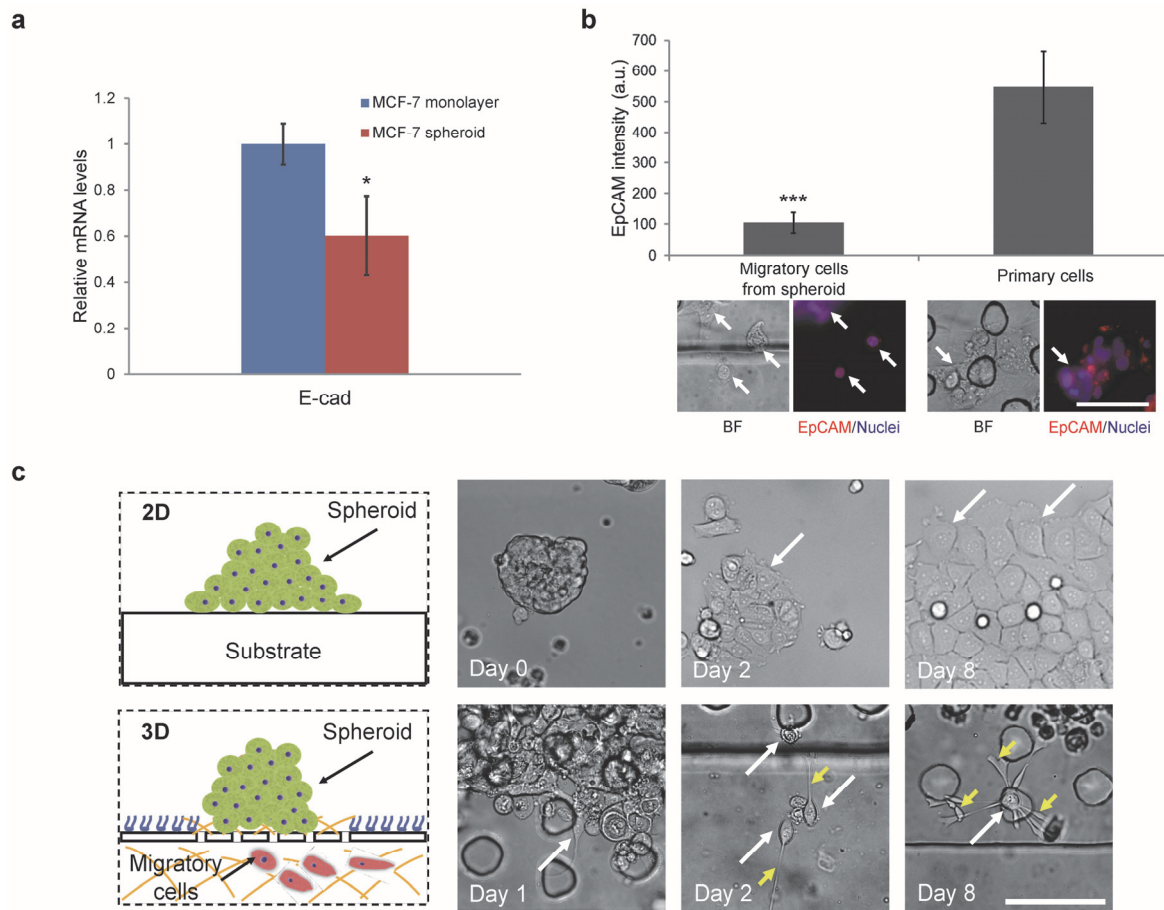


Fig. 5 Phenotypic characteristics of tumor spheroids cultured in the microdevice. (a) Relative expression of mRNAs encoding EMT markers (E-cadherin) in MCF-7 monolayers and MCF-7 spheroids, as evaluated by real-time RT-PCR. GAPDH was used as an internal control and to normalize the variability in sample loading. (b) EpCAM signal intensities from all cells (primary cells in the top channel and migratory cells from spheroids in the bottom channel) were measured. Each point represents an average with $n = 6 \sim 11$. (c) Schematic diagram of cell migration and their relative morphology in 2D and 3D conditions. The top panel shows a spheroid spreading at Day 0, Day 2, and Day 8 in traditional 2.5D cultures. The bottom panel shows migratory cells (indicated by white arrows) at Day 1, Day 2, and Day 8. After one day, single or tether-like cells were observed showing the formation of pseudopodia protrusion (indicated by yellow arrows). Scale bars, 100 μm .